IEEE Photonics Journal
An IEEE Photonics Society Publication

Open Access

Two-Port Noise Suppression in Dual-Polarization Interferometric Fiber-Optic Gyroscope

Volume 11, Number 2, April 2019

Pei Li
Yulin Li
Fangyuan Chen
Chao Peng
Zhengbin Li

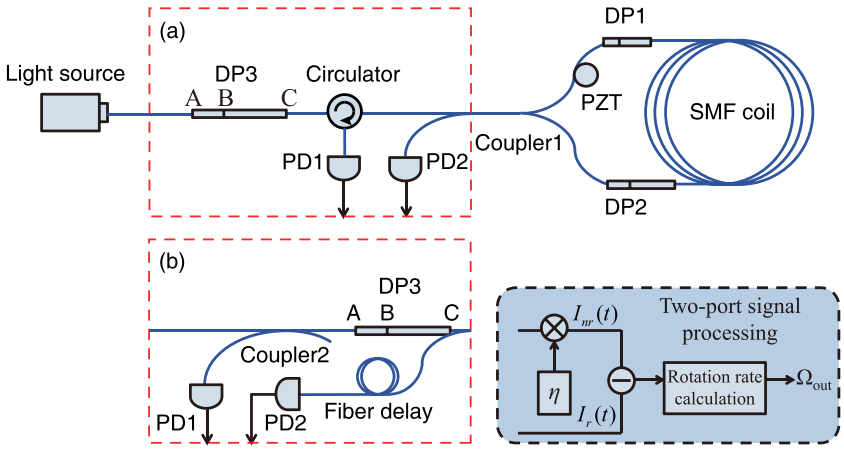

DOI: 10.1109/JPHOT.2019.2908840
1943-0655

Two-Port Noise Suppression in Dual-Polarization Interferometric Fiber-Optic Gyroscope

Pei Li, Yulin Li, Fangyuan Chen, Chao Peng, and Zhengbin Li

State Key Laboratory of Advanced Optical Communication Systems and Networks, School of Electronics Engineering and Computer Science, Peking University, Beijing 100871, China

DOI:10.1109/JPHOT.2019.2908840

Manuscript received February 13, 2019; revised March 24, 2019; accepted March 29, 2019. Date of publication April 2, 2019; date of current version April 16, 2019. This work was supported in part by the National Natural Science Foundation of China under Grant 91736207 and Grant 61575002, and in part by the State Administration for Science, Technology and Industry for National Defense under Grant D020403. Corresponding author: Chao Peng (e-mail: pengchao@pku.edu.cn).

Abstract: Since the polarization non-reciprocity errors are canceled out through optical compensation in dual-polarization interferometric fiber-optic gyroscopes (IFOGs), two ports, namely, the reciprocal and nonreciprocal ports, are both feasible sensing output. In this work, we propose and demonstrate a weighted subtraction method for noise suppression that utilizes the partial correlated two-port signals simultaneously. The relative intensity noise has reduced to 56.2% of its original value in the experiment and agrees with the theoretical analysis; as a result, the angle random walk is suppressed from 5.7×10^{-2} to $3.2 \times 10^{-2}/\sqrt{\text{h}}$ with a 2-km-long fiber. The improvement on short- and long-term stability performance has been experimentally verified, which makes dual-polarization IFOG configuration promising for many applications.

Index Terms: Noise suppression, RIN, dual-polarization, interferometric fiber-optic gyroscope, optical compensation.

1. Introduction

As inertial rotation sensors, interferometric fiber-optic gyroscopes (IFOGs) have been widely utilized in many military and civilization applications owing to their excellent performance in sensitivity and stability [1]. Because the non-reciprocal Sagnac phase shift induced by rotation is ultra-small and easily overwhelmed by the noises [2], the conventional IFOGs require the light propagating in absolute reciprocal paths. As a result, the "minimum configuration" that maintain single polarization to suppress polarization non-reciprocity (PN) errors is proposed and widely adopted in many researches and products [1].

Recently, an alternative configuration denoted as "dual-polarization configuration" is developed for PN error suppressing in which two orthogonal and incoherent polarizations are utilized simultaneously [3]–[7]. Although the PN errors inevitably accompany with both polarizations, they have opposite signs thus can cancel out, or say compensated, optically or electronically. A series of investigation shows that the dual-polarization IFOGs have various benefits in the temperature [8], [9] and magnetic field [10] stability, as well as cost-effectiveness [11].

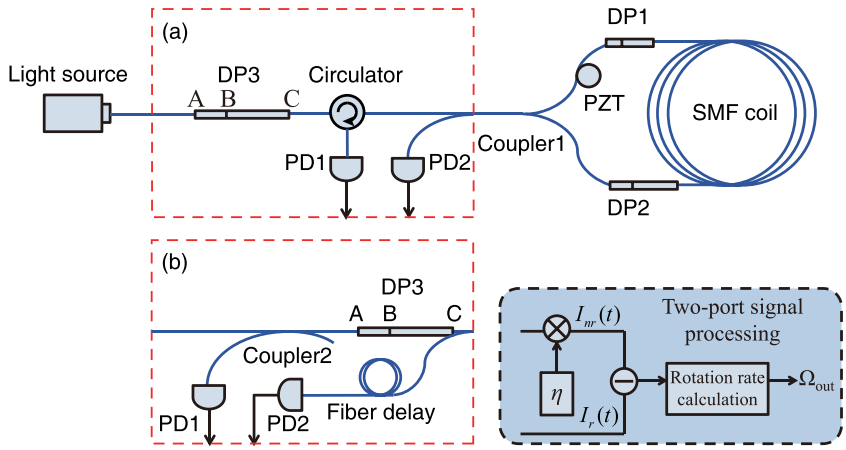

Fig. 1. Schematics of dual-polarization IFOGs. PD: photodetector; PZT: piezoelectric transducer; DP: depolarizer; SMF: single-mode fiber, $I_{r,nr}$: signals detected by PDs, η: weight coefficient, Ω_{out}: the demodulated rotation rate from co-processing two-port signals. (a) A modified setup using circulator. (b) A previous setup [5].

In dual-polarization configuration, one interesting and important fact is that the compensation of PN errors is valid for both reciprocal and non-reciprocal ports [4], [5], [11], [12]. As a result, the conventional non-reciprocal port can also be utilized for rotation sensing except it is biased by a relative stable coupler non-reciprocity (CN) error [11], [13]. This actually re-interprets the meaning of polarization reciprocity. As a result, an ultra-simple IFOG that possess even fewer optical components than "minimum configuration" is demonstrated [11], [12].

Since the two-port (i.e., reciprocal port and conventional non-reciprocal port) outputs the rotation signals simultaneously, it is possible to utilize them together for better noise suppression since the signals come from the same light source and travel through the same sensing coil, and hence, should be correlated to a certain extend.

In this work, we demonstrate an optically compensated IFOG setup which is capable of two-port operation. The correlation between the two-port signals is theoretically modeled and discussed. We found that the short-term noise is dominated by the relative intensity noise (RIN) from the light source. Confirmed by experiment results, the two-port signals are partially correlated since the light spectrum at two individual port is complementary. With weighted subtraction of the two signals, the short-term stability of IFOG is improved. The angle random walk (ARW) is suppressed from $5.7 \times 10^{-2\circ}/\sqrt{\text{h}}$ to $3.2 \times 10^{-2\circ}/\sqrt{\text{h}}$, which is 56.2% of its original value.

2. Theory

2.1 PN Error Suppression

The dual-polarization IFOG setup for this investigation is schematically illustrated in Fig. 1(a), in which Lyot depolarizers (DPs) are adopted to create two orthogonal and incoherent polarizations that travel through a single-mode fiber (SMF) coil. The piezoelectric transducer (PZT) provides sinusoidal phase modulation and we adopt the harmonic demodulation method [14], [15] to obtain the rotation rate. As will elaborate later, two-port, namely the reciprocal port and conventional non-reciprocal port of Coupler1, carry the rotation signals simultaneously and are detected by using two photodetectors (PDs), respectively. The setup of Fig. 1(a) is actually a modified version of our previous configuration of Fig. 1(b), in which DP3 was moved to the front of the circulator in order to improve the correlation of the signals from PD1/2 for better noise suppression.

Under dual-polarization operation, the signals of two orthogonal polarizations x, y at reciprocal and nonreciprocal ports can be written as [5], [11]:

$$I^{r}_{x,y} = I^{r}_{x_0,y_0} + \sqrt{p^2_{rx,ry} + q^2_{rx,ry}}\cos(\phi_s + \Delta\phi_{rx,ry} + \phi_m)$$
$$I^{nr}_{x,y} = I^{nr}_{x_0,y_0} + \sqrt{p^2_{nrx,nry} + q^2_{nrx,nry}}\cos(\phi_s + \phi_c + \Delta\phi_{nrx,nry} + \phi_m). \quad (1)$$

where ϕ_s and ϕ_m are Sagnac phase shift and modulation phase, respectively. The subscripts x and y correspond to the two polarizations, and the scripts r and nr denote the reciprocal and nonreciprocal ports, respectively. The coefficients $p_{rx,ry}$, $q_{rx,ry}$ and $p_{nrx,nry}$, $q_{nrx,nry}$ are given by the system transmission matrices, and hence, the PN errors at two-port are derived as $\Delta\phi_{rx,ry} = \arctan(p_{rx,ry}/q_{rx,ry})$ and $\Delta\phi_{nrx,nry} = \arctan(p_{nrx,nry}/q_{nrx,nry})$ (see the Appendix of Ref. [5] for the details).

Although the non-zero PN errors always accompany with single x, y polarizations, they have opposite polarities and thus can be mutually canceled when summing up the intensity of two polarizations. It is proved by theory and experiments that effective PN error suppression can be achieved when the two orthogonal polarizations are incoherent and balanced in power, and such principle is valid for both reciprocal and nonreciprocal ports (see Appendix for the details). The only difference is that, an extra phase shift $\phi_c \approx \pi$ is induced by the CN at the nonreciprocal port, which induces a relatively stable bias to the output thus can be calibrated.

2.2 Correlation of the Two-Port Signals

Since the two-port outputs the rotation signals simultaneously, we would investigate the possibility of utilizing them together for better noise suppression. The short-term noise of IFOGs mainly consists of three sources [16]–[18]

$$\langle i^2_N \rangle = \langle i^2_I \rangle + \langle i^2_S \rangle + \langle i^2_T \rangle \quad (2)$$

which are the RIN i_I, shot noise i_S, and thermal noise i_T, respectively. More specifically, the thermal noise is given as $\langle i^2_T \rangle = 4kBT/R_L$, which depends on the Boltzmann constant k, temperature T, as well as the detection bandwidth B and resistance R_L. The shot noise is given by $\langle i^2_S \rangle = 2\eta_{QE} eB\langle i \rangle$ with the quantum efficiency η_{QE}, electron charge e and average detection current $\langle i \rangle$.The RIN can be expressed as $\langle i^2_I \rangle = B\langle i \rangle^2/\Delta\nu$ in which $\Delta\nu$ is the bandwidth of the light source [16]. In typical IFOGs, the RIN is one or two orders of magnitude higher than the other two noises [18], therefore, it is the dominate noise in short-term time scale. In physics, the phase fluctuation of broadband light source generate random beatings, i.e. RIN $n_0(t)$, and hence, the intensity can be depicted by $i_I(t) = I_0 + n_0(t)$ which is no longer constant. Due to the insertion loss, only portion of light arrives at the reciprocal and nonreciprocal port outputs, we denote the ratio as α_r and α_{nr} respectively, and the signals detected by the two PDs are:

$$I_r(t) = \alpha_r[I_0 + n_r(t)][1 + k_r\cos(\phi)], \quad (3)$$
$$I_{nr}(t) = \alpha_{nr}[I_0 + n_{nr}(t)][1 - k_{nr}\cos(\phi + \phi_c)]. \quad (4)$$

Here $\phi = \phi_s + \phi_m(t)$, ϕ_s and $\phi_m(t)$ are the Sagnac phase shift and modulated phase, respectively. k_r and k_{nr} are contrast weights, and $n_r(t)$ and $n_{nr}(t)$ are the RINs detected at the two-port. Notice that we take a minus sign of the cos(·) term in Eq. (4) which makes $\phi_c \approx 0$ instead of π. As mentioned, ϕ_c is a steady bias under stable temperature [11], [13].

For harmonic demodulation, the RIN distributes to each harmonic that degrade the sensitivity of IFOG. It is noteworthy that, the RINs at the detected signals differ from the RIN of the light source. As we discussed previously [19]–[21], the birefringence of polarization-maintaining (PM) fiber segments in the SM fiber coil (i.e., the DPs) induce different spectrum ripples at the two-ports, as shown in Fig. 2. As a result, the normalized correlation coefficient γ between $n_r(t)$ and $n_{nr}(t)$ is

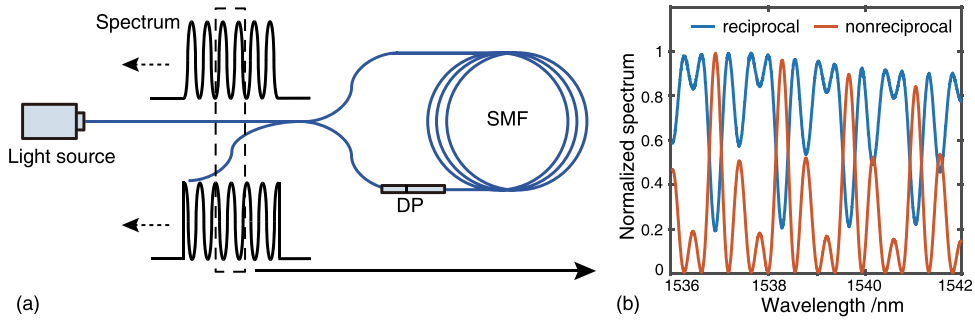

Fig. 2. The light spectra at the output from the reciprocal and nonreciprocal ports. (a) The schematic setup. (b) The measured spectra.

given as [22]–[24]:

$$\gamma(\tau) = \overline{n_r(t)n_{nr}(t-\tau)} = 16\int_0^\infty G_{12}(v)e^{-2\pi jv\tau}\mathrm{d}v\left[\int_0^\infty G_{12}(v)e^{-2\pi jv\tau}\mathrm{d}v\right]^* \tag{5}$$

γ can be directly calculated from the acquired time domain signals $n_r(t)$ and $n_{nr}(t)$, or estimated from the integral of $G_{12}(v)$ which is the mutual light spectral density detected by the PD1/2. Because of the spectrum ripples as shown in Fig. 2(b), the correlation of the two ports signals is reduced to some extent. Nevertheless, they are still partially correlated, then we have:

$$\begin{aligned} In_r(t) &= \rho_r n_0(t) + n_c(t) + n_{1r}(t) \\ n_{nr}(t) &= \rho_{nr} n_0(t) + n_c(t) + n_{1nr}(t) \end{aligned} \tag{6}$$

where $\rho_r n_0(t)$ and $\rho_{nr} n_0(t)$ are the noises correlated with the light source with the correlation coefficient ρ_r and ρ_{nr}. The rest of noises can be divided into two parts, namely, the common-mode component $n_c(t)$ and random independent components $n_{1r}(t)$ and $n_{1nr}(t)$. Therefore, the normalized correlation coefficient γ between $n_r(t)$ and $n_{nr}(t)$ correlation should be at least larger than $\rho_r\rho_{nr}$.

We adopt a weighted subtraction of the two-port signals for noise suppression, as:

$$\begin{aligned} I_{out}(t) &= I_r(t) - \eta I_{nr}(t) \\ &= (\alpha_r - \eta\alpha_{nr})[I_0 + \rho_r n_0(t) + n_c(t)] + I_D(t)\cos(\phi + \phi_N) + n_e(t) \end{aligned} \tag{7}$$

with

$$\begin{aligned} I_D(t) &= [I_0 + \rho_r n_0(t) + n_c(t)]\sqrt{(A_1 + A_2)^2 + A_3^2}, \\ \phi_N &= \arctan[A_3/(A_1 + A_2)], \\ A_1 &= \alpha_r k_r,\ \ A_2 = \eta\alpha_{nr}k_{nr}\cos(\phi_C),\ \ A_3 = \eta\alpha_{nr}k_{nr}\sin(\phi_C). \end{aligned} \tag{8}$$

and

$$n_e(t) = [1 + k_r\cos(\phi)]\alpha_r n_{1r}(t) - [1 - k_{nr}\cos(\phi + \phi_c)]\eta\alpha_{nr}[n_{1nr}(t) + (\rho_{nr} - \rho_r)n_0(t)] \tag{9}$$

Assumed $\rho_{nr} \approx \rho_r$ and we have an ideal 50:50 coupler which gives $k_r = k_{nr} = 0.5$ and perfect subtraction at weight η so that $\alpha_r = \eta\alpha_{nr} = \alpha$; Also noticed that $\phi_C \approx 0$ and $n_{1r}(t)$, $n_{1nr}(t)$ are independent, so we obtained that:

$$\begin{aligned} I_{out}(t) &\approx I_D(t)\cos(\phi + \phi_C/2) + n_e(t) \\ n_e(t) &= \alpha_r[(1 + 0.5\cos(\phi))n_{1r}(t) - (1 - 0.5\cos(\phi))n_{1nr}(t)] \end{aligned} \tag{10}$$

Therefore, the direct components, as well as the correlation part of the RIN, are eliminated. The residual noise, represented by $n_e(t)$, originates from the RINs without correlation. The two-port

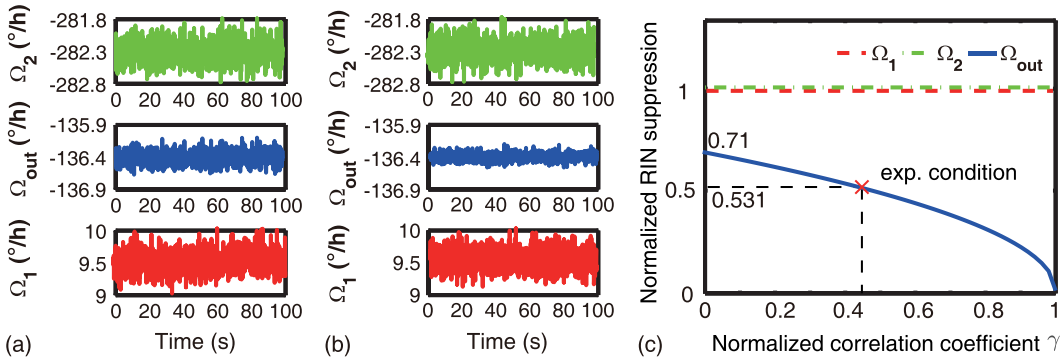

Fig. 3. Simulation results for dual-polarization IFOG outputs with RIN. $\Omega_{1,2}$: rotation rates directly demodulated from PD1, PD2; Ω_{out}: rotation rate demodulated from the weighted subtraction. Time domain signals for normalized correlation coefficient (a) $\gamma = 0.44$ and (b) $\gamma = 0.64$. (c) Normalized RIN suppression for different γ.

operation induces a stable bias of $\phi_C/2$ due to coupler nonreciprocity, which has been proved to have no significant influence on the IFOG stability [5]. By utilizing the signals from the two-ports, the RIN can be suppressed more effectively.

3. Simulations

We perform time domain simulations for the proposed dual-polarization IFOG setup and the results are presented in Fig. 3(a) and (b). We apply simulation parameters that best captures our experiment described in the later section. Specifically, the rotation rate was set to 9.67 $^\circ/$ h in accordance with detecting Earth rotation at our laboratory location of latitude 39.99 $^\circ$N. As will elaborate later, the CN bias of 5.35×10^{-3} rad was obtained in the experiment, and we also add it to the nonreciprocal port in the simulation. The same level of RIN was set for all simulations, with a signal-to-noise ratio (SNR) of 65 dB. The sampling interval was 0.1 s and the simulation was performed for 100 s.

For the results shown in Fig. 3(a), the normalized correlation coefficient γ was set to approximately 0.44 which is almost equivalent to our experimental observation. Compared with the rotation rates obtained at the reciprocal and nonreciprocal ports, namely, Ω_1 and Ω_2, respectively, the short-term noise was effectively reduced for the final output Ω_{out} by using weighted subtraction. The RIN was suppressed to 53.1% of its original value for $\gamma = 0.44$. More significant noise suppression can be achieved if the two-port signals are more correlated. As illustrated in Fig. 3(b), the RIN was suppressed to 42.4% for $\gamma = 0.64$.

The effectiveness of noise suppression is highly related to the correlation of the two-port signals. A more detailed simulation was performed to determine the RIN suppression ratio under different γ, as shown in Fig. 3(c). We keep the same level of the RIN and the short-term noise on rotation rate outputs was normalized by that of the reciprocal port. Even $n_r(t)$ and $n_{nr}(t)$ were completely independent, the noise under weighted subtraction was 71% that of the original two outputs. For strong correlated $n_r(t)$ and $n_{nr}(t)$, most of the RIN can be canceled. In other words, the proposed method is especially useful when γ is large, as apparent from Fig. 3(c).

4. Experiment

We also experimentally verify the effectiveness of the two-port noise suppression method. In the experiment, an amplified spontaneous emission (ASE) light source with a center wavelength of 1550 nm and a bandwidth of 70 nm was used. The decoherence length was calculated as $L_{dc} = 34$ μm. The refractive index difference between the fast and slow axes of the PMF in the DPs was $\Delta n = 5 \times 10^{-4}$. To depolarize the source, the length of $\overline{AB}$ in DP3 was required to be longer

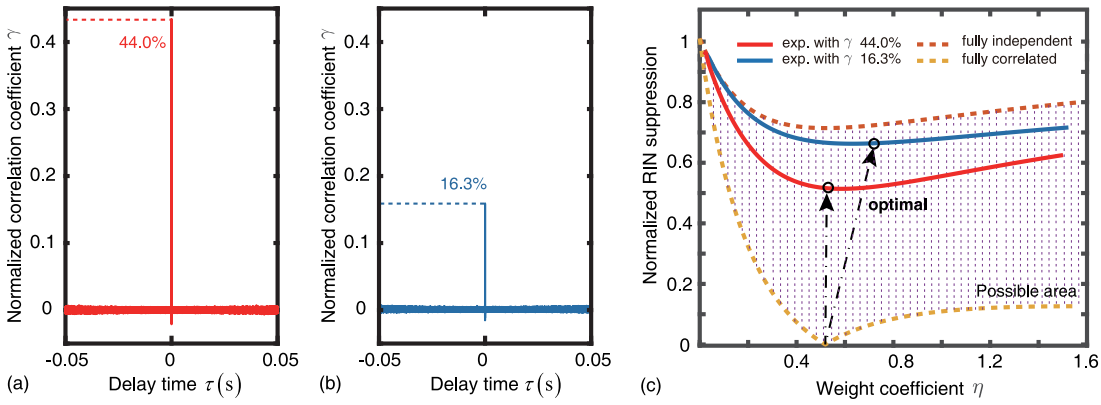

Fig. 4. Normalized correlation coefficients calculated from time domain signals for (a) the modified setup presented in Fig. 1(a) and (b) the previous setup presented in Fig. 1(b). (c) Normalized RIN suppression vs. different weight coefficient η.

than $L_{dp} = L_{dc}/\Delta n = 0.068$m. The coil length, coil diameter, and fiber core diameter were 2000 m, 0.14 m, and 125 μ m, respectively. To cancel the random birefringence in this coil, a DP length of $L'_{dp} = 1.25$ m was required [25]. We used a redundant depolarizing length $L'_0 = 2.0$ m instead of $L'_{dp} = 1.25$ m. Accordingly, the lengths of the $\overline{AB}$ parts in DP1, DP2, and DP3 were chosen to be 2, 8, and 32 m, respectively. Therefore, DP3 could effectively depolarize the source. Every $\overline{BC}$ length was twice the length of the connected $\overline{AB}$. In practical applications, temperature changes influence the stability of the PMF length and Δn [26]. Therefore, in our design, the lengths were redundant to ensure that the orthogonal polarizations obtained from a DP were always incoherent under our laboratory temperature range. Therefore, the IFOG avoided the influence of PMF instability related to temperature.

The experiments were conducted under an uncontrolled room temperature (15 $\sim$ 25 °C). Note that the Earth's rotation rate is approximately 9.67 °/ h at our laboratory. The digitizer used in the experiments had a sampling rate of 2 MSPS. The IFOG operation at open-loop configuration and harmonic demodulation method is adopted to obtain the rotation rate.

The correlation coefficients are calculated directly from the time-domain signals that acquired from the two-port, and the results for our modified setup Fig. 1(a) and previous setup Fig. 1(b) are illustrated in Fig. 4(a) and (b), respectively. The modified setup achieves better correlation (44%) than the previous one (16.3%), mainly because we adopt a circulator to pick up the reciprocal port signal before its re-entrance into DP3 that modifies the light spectrum and lowers the correlation.

The effectiveness of noise suppression also depends on the weight subtraction coefficient η. As shown in Fig. 4(c), there exist an optimal weight coefficient for best noise suppression, when the correlation coefficient γ is given. Under the conditions that the independent noises $n_{1r}(t)$, $n_{1nr}(t)$ are sufficient small, or say the two-port signals are highly correlated, the optimal weight approaches to the power balance case $\rho_r = \rho_{nr}$, which gives $\eta = 0.5$ in theory. The red and yellow lines indicate two extreme scenarios that $n_r(t)$ and $n_{nr}(t)$ are completely independent and correlated, respectively, which sets up a possible area of the proposed method. The optimal weight η depends on the optical structure and the power ratio between the two-port, which is a constant number once the IFOG setup was assembled. In experiment, we demodulate the rotation signal with a series of η in order to find the optimal one that minimizes the ARW, as shown in Fig. 4(c). For our previous setup of Fig. 1(b), we have the correlation coefficient $\gamma = 0.163$ which results in suppressed noise ratio of 66.7% when the optimal coefficient $\eta = 0.71$ is adopted. In this case, it is noteworthy that $\eta \neq 0.5$ because $\rho_r \neq \rho_{nr}$. The correlation coefficient increases to $\gamma = 0.44$ for the modified setup of Fig. 1(a), and hence, a better noise ratio of 56.2% has been achieved with optimal $\eta = 0.5$.

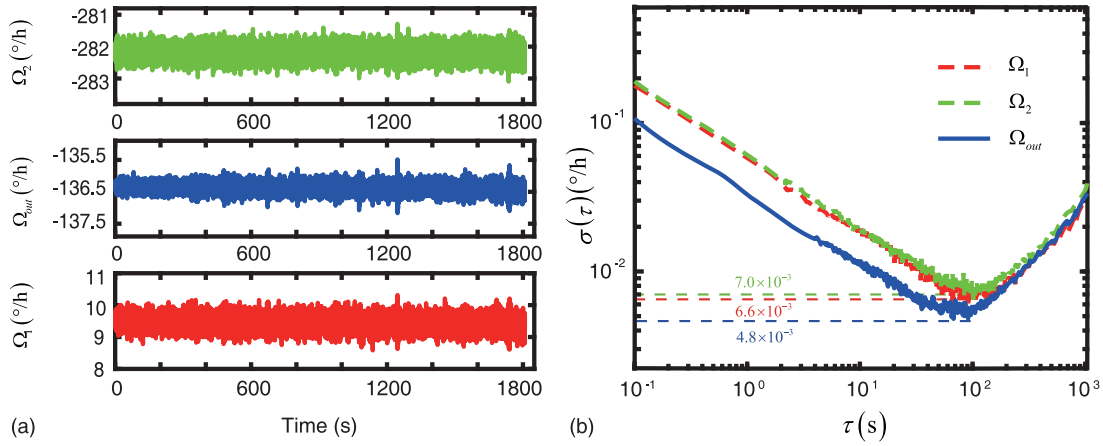

Fig. 5. Experiment results for IFOG outputs with the modified setup of Fig. 1(a). (a) Rotation rate in time domain. (b) Allan variance analysis of IFOG outputs.

TABLE 1
Allan Variance Indices of IFOG

	Ω_1	Ω_2	Ω_{out}
ARW($^\circ/\sqrt{\text{h}}$)	5.7×10^{-2}	6.0×10^{-2}	3.2×10^{-2}
BI ($^\circ$/h)	6.6×10^{-3}	7.0×10^{-3}	4.8×10^{-3}

For the setup of Fig. 1(a), the time domain signals are recorded with an integration time of 0.35 s and a test duration of 30 min, as shown in Fig. 5(a). Hence, we can intuitively observe that output applied with optimal weight coefficient $\eta = 0.5$ features less short-term noise than any of the direct outputs Ω_1 or Ω_2. Besides, the bias in Ω_{out} was approximately half the CN bias in Ω_2, which was observed in both the experiments and simulations. The bias was stable, therefore, can be calibrated. For instance, the CN bias can be extracted by linear least squares fitting the demodulated signals with the angular velocities of the rotary table, or the tilted angles when inclining the IFOG. In this work, CN bias was determiend as 5.35×10^{-3} rad. As verified previously [5], the CN bias would not seriously degrade the stability performance of IFOG when an appropriate initial calibration method is adopted.

We performed Allan variance analysis to conduct a detailed comparison of the effectiveness of noise suppression [27], as shown in Fig. 5(b). The Allan curve of the weighted subtraction output was consistently lower than those for the two directly demodulated ones, especially for the short-term region. The ARW and bias instability (BI) noise indices of the experiment results are listed in Table 1. The ARW was suppressed from $5.7 \times 10^{-2\circ}/\sqrt{\text{h}}$ to $3.2 \times 10^{-2\circ}/\sqrt{\text{h}}$ and the BI was suppressed from $6.6 \times 10^{-3\circ}$/h to $4.8 \times 10^{-3\circ}$/h. Both the short- and long-term noises indices were improved by the proposed method, especially for the short-term ones. The RIN was suppressed to 56.2% of the original value, agrees with the simulation result of 53.1%.

Above experiments verify the validity of co-utilizing the partially correlated two-port signals in dual-polarization IFOG for better noise suppression. The effectiveness of the proposed method is particularly evident in short-term time scale. For long-term instability, such method still works but the optimal weight may vary slowly with temperature and needs updating in real-time. The proposed method can also combine with other sophisticated signal processing methods [28], [29] to further improve the performance, which makes dual-polarization IFOG configuration promising for many applications.

TABLE 2
Derivation Results for Dual-Polarization IFOGs

	Reciprocal port	Nonreciprocal port
p_x	$-(1-d)A_{r23}sin\phi_{r23}$	$(1-d)A_{nr23}sin\phi_{nr23}$
q_x	$(1+d)\|C_{r1}\|^2+(1-d)A_{r23}cos\phi_{r23}$	$-(1+d)\|C_{nr1}\|^2+(1-d)A_{nr23}cos\phi_{nr23}$
p_y	$(1+d)A_{r23}sin\phi_{r23}$	$-(1+d)A_{nr23}sin\phi_{nr23}$
q_y	$(1-d)\|C_{r4}\|^2+(1+d)A_{r23}cos\phi_{r23}$	$-(1-d)\|C_{nr1}\|^2+(1+d)A_{nr23}cos\phi_{nr23}$
A_{23}	$\|C_{r2}C_{r3}\|\Gamma(z_{23})$	$\|C_{nr2}C_{nr3}\|\Gamma(z_{23})$

5. Conclusion

In this work, we proposed and demonstrated a weighted subtraction method for noise suppression, based on the correlation characteristics of the two-port signals in dual-polarization IFOG. We derived the noise model at the two-port signals and found an optimal weight coefficient for best noise suppression. The correlated portion of noise appeared at reciprocal and nonreciprocal ports mutually cancels out, and the RIN has reduced to 56.2% of its original value in the experiment. The ARW was suppressed from $5.7\times10^{-2}{}^\circ/\sqrt{\text{h}}$ to $3.2\times10^{-2}{}^\circ/\sqrt{\text{h}}$ and the BI was suppressed from $6.6\times10^{-3}{}^\circ$/h to $4.8\times10^{-3}{}^\circ$/h, which validates the effectiveness of the proposed two-port noise suppression method.

Appendix

In dual-polarization IFOGs, the intensity of the two orthogonal polarizations is summed up directly at the PD, which we refer it as to "optical compensation." Assuming the two polarization are incoherent, the PN errors at reciprocal and nonreciprocal ports can be expressed as [5], [30]

$$\Delta\phi_r = \arctan\frac{p_{rx}+p_{ry}}{q_{rx}+q_{ry}} = \arctan\frac{2d|C_{r2}C_{r3}|\Gamma(z_{23})\sin\phi_{r23}}{|C_{r1}|^2(1+d)+|C_{r4}|^2(1-d)+2|C_{r2}C_{r3}|\Gamma(z_{23})\cos\phi_{r23}}$$
$$\Delta\phi_{nr} = \arctan\frac{p_{nrx}+p_{nry}}{q_{nrx}+q_{nry}} = \arctan\frac{2d|C_{nr2}C_{nr3}|\Gamma(z_{23})\sin\phi_{nr23}}{|C_{nr1}|^2(1+d)+|C_{nr4}|^2(1-d)+2|C_{nr2}C_{nr3}|\Gamma(z_{23})\cos\phi_{nr23}} \tag{11}$$

where $p_{rx,ry}$, $q_{rx,ry}$ and $p_{nrx,nry}$, $q_{nrx,nry}$ are listed in Table 2; d is the degree of depolarization (DOP) before entering the loop; note that $d=0$ for well depolarized light. Furthermore, C_{r1} (C_{nr1}) and C_{r4} (C_{nr4}) are diagonal terms and C_{r2} (C_{nr2}) and C_{r3} (C_{nr3}) are off-diagonal terms of the transmission matrices for counter-propagating beams meeting at the reciprocal port (nonreciprocal port); these coefficients are complex numbers. $\Gamma(z_{23})$ is the degree of coherence of the light source [31], where z_{23} represents the birefringent delay induced by $C_{r2}C_{r3}^*$ ($C_{nr2}C_{nr3}^*$). Finally, ϕ_{r23} (ϕ_{nr23}) is the phase of $C_{r1}C_{r4}^*$ ($C_{nr1}C_{nr4}^*$). Therefore, when $d\approx0$, namely two orthogonal polarization are balanced in power, the PN errors of the two polarizations cancel each other at the reciprocal port as well as nonreciprocal port, i.e. $\Delta\phi_r\approx0$ and $\Delta\phi_{nr}\approx0$. Thus, the reciprocal port and the nonreciprocal port can be both feasibly employed as sensing outputs.

Acknowledgment

The authors wish to thank Zinan Wang and Rongya Luo for their valuable comments and the anonymous reviewers for their valuable suggestions.

References

[1] H. C. Lefevre, *The Fiber-Optic Gyroscope*. Norwood, MA, USA: Artech house, 2014.
[2] E. J. Post, "Sagnac effect," *Rev. Mod. Phys.*, vol. 39, no. 2, pp. 475–493, 1967.

[3] Y. Yang, Z. Wang, and Z. Li, "Optically compensated dual-polarization interferometric fiber-optic gyroscope," *Opt. Lett.*, vol. 37, no. 14, pp. 2841–2843, 2012.
[4] Z. Wang *et al.*, "All-depolarized interferometric fiber-optic gyroscope based on optical compensation," *IEEE Photon. J.*, vol. 6, no. 1, Feb. 2014, Art. no. 7100208.
[5] Z. Wang *et al.*, "Optically compensated polarization reciprocity in interferometric fiber-optic gyroscopes," *Opt. Exp.*, vol. 22, no. 5, pp. 4908–4919, 2014.
[6] R. Luo, Y. Li, S. Deng, C. Peng, and Z. Li, "Effective suppression of residual coherent phase error in a dual-polarization fiber optic gyroscope," *Opt. Lett.*, vol. 43, no. 4, pp. 815–818, 2018.
[7] Y. Li *et al.*, "Suppressing polarization non-reciprocity error with reverse phase modulation in dual-polarization fiber optic gyroscopes," *Opt. Exp.*, vol. 26, no. 26, pp. 34150–34160, 2018.
[8] P. Lu, Z. Wang, R. Luo, D. Zhao, C. Peng, and Z. Li, "Polarization nonreciprocity suppression of dual-polarization fiber-optic gyroscope under temperature variation," *Opt. Lett.*, vol. 40, no. 8, pp. 1826–1829, 2015.
[9] R. Luo, Y. Li, S. Deng, D. He, C. Peng, and Z. Li, "Compensation of thermal strain induced polarization nonreciprocity in dual-polarization fiber optic gyroscope," *Opt. Exp.*, vol. 25, no. 22, pp. 26747–26759, 2017.
[10] P. Liu, X. Li, X. Guang, Z. Xu, W. Ling, and H. Yang, "Drift suppression in a dual-polarization fiber optic gyroscope caused by the Faraday effect," *Opt. Commun.*, vol. 394, pp. 122–128, 2017.
[11] F. Chen *et al.*, "Cost effective dual-polarization interferometric fiber optic gyroscope with ultra-simple configuration," in *Proc. Conf. Lasers Electro-Opt.: Appl. Technol.*, 2018, Paper JW2A-172.
[12] Z. Wang *et al.*, "Dual-polarization interferometric fiber-optic gyroscope with an ultra-simple configuration," *Opt. Lett.*, vol. 39, no. 8, pp. 2463–2466, 2014.
[13] G. Keiser, *Optical Fiber Communications*. New York, NY, USA: McGraw-Hill, 2008.
[14] R. A. Bergh, H. C. Lefevre, and H. J. Shaw, "All-single-mode fiber-optic gyroscope with long-term stability," *Opt. Lett.*, vol. 6, no. 10, pp. 502–504, 1981.
[15] Y. Gronau and M. Tur, "Digital signal processing for an open-loop fiber-optic gyroscope," *Appl. Opt.*, vol. 34, no. 25, pp. 5849–5853, 1995.
[16] R. C. Rabelo, R. T. de Carvalho, and J. Blake, "SNR enhancement of intensity noise-limited FOGs," *J. Lightw. Technol.*, vol. 18, no. 12, pp. 2146–2150, Dec. 2000.
[17] Y. Li, Z. Wang, Y. Yang, C. Peng, Z. Zhang, and Z. Li, "A multi-frequency signal processing method for fiber-optic gyroscopes with square wave modulation," *Opt. Exp.*, vol. 22, no. 2, pp. 1608–1618, 2014.
[18] F. Guattari, C. Molucon, A. Bigueur, E. Ducloux, and H. Lefevre, "Touching the limit of fog angular random walk: Challenges and applications," in *Proc. DGON Intertial Sens. Syst.*, 2016, pp. 1–13.
[19] X. Fang, "A variable-loop Sagnac interferometer for distributed impact sensing," *J. Lightw. Technol.*, vol. 14, no. 10, pp. 2250–2254, Oct. 1996.
[20] X. Dong, H. Tam, and P. Shum, "Temperature-insensitive strain sensor with polarization-maintaining photonic crystal fiber based Sagnac interferometer," *Appl. Phys. Lett.*, vol. 90, no. 15, 2007, Art. no. 151113.
[21] B. Song *et al.*, "Highly sensitive twist sensor employing Sagnac interferometer based on PM-elliptical core fibers," *Opt. Exp.*, vol. 23, no. 12, pp. 15372–15379, 2015.
[22] Y. Li, F. Ben, R. Luo, C. Peng, and Z. Li, "Excess relative intensity noise suppression in depolarized interferometric fiber optic gyroscopes," *Opt. Commun.*, vol. 440, pp. 83–88, 2019.
[23] M. Born and E. Wolf, *Principles of Optics*, 7th ed. Cambridge, U.K.: Cambridge Univ. Press, 1999.
[24] J. W. Goodman, *Statistical Optics*. Hoboken, NJ, USA: Wiley, 2000.
[25] R. Ulrich, S. Rashleigh, and W. Eickhoff, "Bending-induced birefringence in single-mode fibers," *Opt. Lett.*, vol. 5, no. 6, pp. 273–275, 1980.
[26] D.-H. Kim and J. U. Kang, "Sagnac loop interferometer based on polarization maintaining photonic crystal fiber with reduced temperature sensitivity," *Opt. Exp.*, vol. 12, no. 19, pp. 4490–4495, 2004.
[27] *IEEE Standard Specification Format Guide and Test Procedure for Single-Axis Interferometric Fiber Optic Gyros*, IEEE Standard 952-1997, 1998.
[28] Y. Yang, Z. Wang, and Z. Li, "Unbiasedness of simultaneous independent measurement," *Meas. Sci. Technol.*, vol. 23, no. 8, 2012, Art. no. 085005.
[29] Y. Yang, Z. Wang, C. Peng, and Z. Li, "Multidimensional gray-wavelet processing in interferometric fiber-optic gyroscopes," *Meas. Sci. Technol.*, vol. 24, no. 11, 2013, Art. no. 115203.
[30] Z. Wang, "Output properties of dual-polarization IFOGs," in *Dual-Polarization Two-Port Fiber-Optic Gyroscope*. New York, NY, USA: Springer, 2017, pp. 39–63.
[31] B. Szafraniec and G. A. Sanders, "Theory of polarization evolution in interferometric fiber-optic depolarized gyros," *J. Lightw. Technol.*, vol. 17, no. 4, pp. 579–590, Apr. 1999.